

Beam spin asymmetry in semi-inclusive electroproduction of a hadron pair

M. Mirazita,¹⁹ H. Avakian,⁴² A. Courtoy,¹⁵ S. Pisano,⁵ S. Adhikari,¹³ M.J. Amaryan,³⁵ G. Angelini,¹⁶ H. Atac,⁴¹ N.A. Baltzell,⁴² L. Barion,¹⁸ M. Battaglieri,^{42,20} I. Bedlinskiy,³¹ F. Benmokhtar,¹⁰ A. Bianconi,^{45,23} A.S. Biselli,^{11,3} F. Bossù,⁶ S. Boiarinov,⁴² W.J. Briscoe,¹⁶ W.K. Brooks,^{43,42} D. Bulumulla,³⁵ V.D. Burkert,⁴² D.S. Carman,⁴² J.C. Carvajal,¹³ A. Celentano,²⁰ P. Chatagnon,²⁴ T. Chetry,³⁰ G. Ciullo,^{18,12} B. Clary,⁸ P.L. Cole,^{28,42} M. Contalbrigo,¹⁸ V. Crede,¹⁴ A. D'Angelo,^{21,38} N. Dashyan,⁵¹ R. De Vita,²⁰ M. Defurne,⁶ A. Deur,⁴² S. Diehl,⁸ C. Dilks,⁹ C. Djalali,^{34,40} R. Dupre,²⁴ H. Egiyan,⁴² M. Ehrhart,¹ A. El Alaoui,⁴³ L. El Fassi,³⁰ P. Eugenio,¹⁴ S. Fegan,⁴⁷ R. Fersch,^{7,50} A. Filippi,²² T.A. Forest,¹⁷ Y. Ghandilyan,⁵¹ G. Gavalian,^{42,32} G.P. Gilfoyle,³⁷ K.L. Giovanetti,²⁶ F.X. Girod,⁴² D.I. Glazier,⁴⁶ E. Golovatch,³⁹ R.W. Gothe,⁴⁰ K.A. Griffioen,⁵⁰ M. Guidal,²⁴ L. Guo,^{13,42} K. Hafidi,¹ H. Hakobyan,^{43,51} M. Hattawy,³⁵ T.B. Hayward,⁵⁰ D. Heddle,^{7,42} K. Hicks,³⁴ A. Hobart,²⁴ M. Holtrop,³² Q. Huang,⁶ Y. Ilieva,^{40,16} D.G. Ireland,⁴⁶ B.S. Ishkhanov,³⁹ E.L. Isupov,³⁹ D. Jenkins,⁴⁸ H.S. Jo,^{27,24} K. Joo,⁸ D. Keller,⁴⁹ A. Khanal,¹³ M. Khandaker,^{33,*} C.W. Kim,¹⁶ W. Kim,²⁷ F.J. Klein,⁴ V. Kubarovskiy,^{42,36} S.E. Kuhn,³⁵ L. Lanza,²¹ M. Leali,^{45,23} P. Lenisa,^{18,12} K. Livingston,⁴⁶ I. J. D. MacGregor,⁴⁶ D. Marchand,²⁴ N. Markov,^{42,8} L. Marsicano,²⁰ V. Mascagna,^{44,23,†} B. McKinnon,⁴⁶ R.G. Milner,²⁹ T. Mineeva,⁴³ V. Mokeev,^{42,39} C. Mullen,²⁰ C. Munoz Camacho,²⁴ K. Neupane,⁴⁰ G. Niculescu,^{26,34} T. O'Connell,⁸ M. Osipenko,²⁰ M. Paolone,⁴¹ L.L. Pappalardo,^{18,12} R. Paremuzyan,⁴² K. Park,^{27,‡} E. Pasyuk,⁴² W. Phelps,⁷ D. Pocanic,⁴⁹ O. Pogorelko,³¹ J. Poudel,³⁵ Y. Prok,^{35,49} B.A. Raue,^{13,42} M. Ripani,²⁰ J. Ritman,²⁵ A. Rizzo,^{21,38} P. Rossi,^{42,19} F. Sabatié,⁶ C. Salgado,³³ A. Schmidt,¹⁶ R.A. Schumacher,³ Y.G. Sharabian,⁴² U. Shrestha,³⁴ O. Soto,¹⁹ N. Sparveris,⁴¹ S. Stepanyan,⁴² I.I. Strakovsky,¹⁶ S. Strauch,^{40,16} N. Tyler,⁴⁰ M. Ungaro,^{42,36} L. Venturelli,^{45,23} H. Voskanyan,⁵¹ A. Vossen,⁹ E. Voutier,²⁴ D. Watts,⁴⁷ K. Wei,⁸ X. Wei,⁴² M.H. Wood,^{2,40} B. Yale,⁵⁰ N. Zachariou,⁴⁷ J. Zhang,⁴⁹ and Z.W. Zhao⁹

(The CLAS Collaboration)

¹*Argonne National Laboratory, Argonne, Illinois 60439*

²*Canisius College, Buffalo, NY*

³*Carnegie Mellon University, Pittsburgh, Pennsylvania 15213*

⁴*Catholic University of America, Washington, D.C. 20064*

⁵*Centro Fermi - Museo Storico della Fisica e Centro Studi e Ricerche "Enrico Fermi", Rome, Italy*

⁶*IRFU, CEA, Université Paris-Saclay, F-91191 Gif-sur-Yvette, France*

⁷*Christopher Newport University, Newport News, Virginia 23606*

⁸*University of Connecticut, Storrs, Connecticut 06269*

⁹*Duke University, Durham, North Carolina 27708-0305*

¹⁰*Duquesne University, 600 Forbes Avenue, Pittsburgh, PA 15282*

¹¹*Fairfield University, Fairfield CT 06434*

¹²*Universita' di Ferrara , 44121 Ferrara, Italy*

¹³*Florida International University, Miami, Florida 33199*

¹⁴*Florida State University, Tallahassee, Florida 32306*

¹⁵*Instituto de Física, Universidad Nacional Autónoma de México Apartado Postal 20-364, Ciudad de México 01000, México*

¹⁶*The George Washington University, Washington, DC 20052*

¹⁷*Idaho State University, Pocatello, Idaho 83209*

¹⁸*INFN, Sezione di Ferrara, 44100 Ferrara, Italy*

¹⁹*INFN, Laboratori Nazionali di Frascati, 00044 Frascati, Italy*

²⁰*INFN, Sezione di Genova, 16146 Genova, Italy*

²¹*INFN, Sezione di Roma Tor Vergata, 00133 Rome, Italy*

²²*INFN, Sezione di Torino, 10125 Torino, Italy*

²³*INFN, Sezione di Pavia, 27100 Pavia, Italy*

²⁴*Université Paris-Saclay, CNRS/IN2P3, IJCLab, 91405 Orsay, France*

²⁵*Institute fur Kernphysik (Juelich), Juelich, Germany*

²⁶*James Madison University, Harrisonburg, Virginia 22807*

²⁷*Kyungpook National University, Daegu 41566, Republic of Korea*

²⁸*Lamar University, 4400 MLK Blvd, PO Box 10009, Beaumont, Texas 77710*

²⁹*Massachusetts Institute of Technology, Cambridge, Massachusetts 02139-4307*

³⁰*Mississippi State University, Mississippi State, MS 39762-5167*

³¹*National Research Centre Kurchatov Institute - ITEP, Moscow, 117259, Russia*

³²*University of New Hampshire, Durham, New Hampshire 03824-3568*

³³*Norfolk State University, Norfolk, Virginia 23504*

³⁴*Ohio University, Athens, Ohio 45701*

³⁵*Old Dominion University, Norfolk, Virginia 23529*

³⁶*Rensselaer Polytechnic Institute, Troy, New York 12180-3590*

³⁷ University of Richmond, Richmond, Virginia 23173

³⁸ Universita' di Roma Tor Vergata, 00133 Rome Italy

³⁹ Skobeltsyn Institute of Nuclear Physics, Lomonosov Moscow State University, 119234 Moscow, Russia

⁴⁰ University of South Carolina, Columbia, South Carolina 29208

⁴¹ Temple University, Philadelphia, PA 19122

⁴² Thomas Jefferson National Accelerator Facility, Newport News, Virginia 23606

⁴³ Universidad Técnica Federico Santa María, Casilla 110-V Valparaíso, Chile

⁴⁴ Università degli Studi dell'Insubria, 22100 Como, Italy

⁴⁵ Università degli Studi di Brescia, 25123 Brescia, Italy

⁴⁶ University of Glasgow, Glasgow G12 8QQ, United Kingdom

⁴⁷ University of York, York YO10 5DD, United Kingdom

⁴⁸ Virginia Tech, Blacksburg, Virginia 24061-0435

⁴⁹ University of Virginia, Charlottesville, Virginia 22901

⁵⁰ College of William and Mary, Williamsburg, Virginia 23187-8795

⁵¹ Yerevan Physics Institute, 375036 Yerevan, Armenia

(Dated: October 20, 2020)

A first measurement of the longitudinal beam spin asymmetry A_{LU} in the semi-inclusive electro-production of pairs of charged pions is reported. A_{LU} is a higher-twist observable and offers the cleanest access to the nucleon twist-3 parton distribution function $e(x)$. Data have been collected in the Hall-B at Jefferson Lab by impinging a 5.498-GeV electron beam on a liquid-hydrogen target, and reconstructing the scattered electron and the pion pair with the CLAS detector. One-dimensional projections of the $A_{LU}^{\sin\phi_R}$ moments are extracted for the kinematic variables of interest in the valence quark region. The understanding of di-hadron production is essential for the interpretation of observables in single hadron production in semi-inclusive DIS, and pioneering measurements of single spin asymmetries in di-hadron production open a new avenue in studies of QCD dynamics.

PACS numbers: 12.38.-t, 13.40.-f, 13.60.-r, 25.30.-c, 25.30.Rw, 25.30.Dh, 25.30.Fj

The correlations between quarks and gluons occurring inside the nucleon play an essential role in QCD dynamics. Asymmetries from semi-inclusive deep inelastic scattering (SIDIS), where a highly virtual photon interacts with a hadronic target and at least one hadron is detected in the final state, have appeared to be effective tools to access quark distributions and fragmentation information. Studies of hadron pairs in SIDIS open qualitatively new possibilities to study QCD dynamics, providing access to correlations not accessible with single hadron SIDIS. The interpretation of di-hadron production in SIDIS, as well as interpretation of single-hadron production, are intimately related to contributions to those samples from correlated di-hadrons in general, and vector mesons, in particular.

At the energy of fixed-target facilities, contributions of order $\mathcal{O}(M/Q)$, with M the target mass and Q^2 the photon virtuality, become sizeable and, therefore, relevant. Such contributions are labeled *twist-3* effects, and can encode quark-gluon correlations.

In the collinear framework—in which we shall work in this letter—six Parton Distribution Functions (PDFs) describe the nucleon up to the twist-3 level. The three leading-twist functions are the unpolarized $f_1(x)$, the helicity $g_1(x)$ and the transversity $h_1(x)$ distributions, where

x is the Bjorken scaling variable. The twist-3 PDFs are $e(x)$, $h_L(x)$ and $g_T(x)$, which describe quark-quark and quark-gluon correlations, and as such have no probabilistic interpretation.

Higher-twist PDFs offer fascinating doorways to study the nucleon beyond its valence structure. An essential role is played by the *chiral-odd* PDF $e(x)$, that is related to the nucleon *scalar charge*—poorly determined through phenomenology—and *a fortiori* to the pion-nucleon sigma term [1]. In addition, it encodes information on the quark mass, as well as genuine quark-gluon correlations [2]. The latter has also been related to an average transverse force acting on a transversely polarized quark in an unpolarized target after the interaction with the virtual photon [3]. It has recently been suggested that this effect could be related to the CP-violating sigma terms [4]. Consequently, the precise measurement of the PDF $e(x)$ could play an important role in searches for Beyond-the-Standard-Model fundamental scalar interactions [5], in the same way the tensor charge does [6].

Measurements of twist-3 observables are available from HERMES [7], CLAS [8–10] and COMPASS [11] for single-pion SIDIS, for which the PDF $e(x)$ is accessible only when the transverse momentum of the final hadron is not integrated out. A first extraction of the –transverse momentum dependent— $e(x)$ PDF has been pursued from the CLAS data [12]. Two-hadron SIDIS measurements provide a method to access twist-3 observables in the collinear framework.

In this letter, we present the first measurement of the beam spin asymmetry (BSA) in the SIDIS electropro-

* Current address: Idaho State University, Pocatello, Idaho 83209

† Current address: Università degli Studi di Brescia, 25123 Brescia, Italy

‡ Current address: Thomas Jefferson National Accelerator Facility, Newport News, Virginia 23606

duction of two charged pions using the CLAS data. The BSA is defined as the ratio between the difference and the sum of the cross sections corresponding to the two beam-helicity states and can be expressed in terms of harmonics in the azimuthal angle ϕ_R , defined below. The $\sin \phi_R$ moment of the BSA can be written as

$$A_{LU}^{\sin \phi_R} = \sqrt{2\epsilon(1-\epsilon)} \frac{F_{LU}^{\sin \phi_R}}{F_{UU,T} + \epsilon F_{UU,L}} , \quad (1)$$

with ϵ the ratio of longitudinal to transverse photon flux, and the structure functions (SFs) [13]

$$\begin{aligned} F_{LU}^{\sin \phi_R} &= - \sum_q e_q^2 x \frac{|\mathbf{R}| \sin \theta}{Q} \\ &\left[\frac{M}{m_{\pi^+\pi^-}} x e^q(x) H_1^{\triangleleft q}(z, \cos \theta, m_{\pi^+\pi^-}) \right. \\ &\left. + \frac{1}{z} f_1^q(x) \tilde{G}^{\triangleleft q}(z, \cos \theta, m_{\pi^+\pi^-}) \right], \end{aligned} \quad (2)$$

$$F_{UU,T} = \sum_q e_q^2 x f_1^q(x) D_1^q(z, \cos \theta, m_{\pi^+\pi^-}), \quad (3)$$

$$F_{UU,L} = 0, \quad (4)$$

contain a sum over the quark flavors q with charge e_q , with M the target mass and $m_{\pi^+\pi^-}$ the invariant mass of the pion pair. The angles are calculated in the center-of-mass frame of the virtual photon-proton system. We define the sum of the two pion momenta $\mathbf{P}_h = \mathbf{P}_{\pi^+} + \mathbf{P}_{\pi^-}$ as well as their half-difference $\mathbf{R} = (\mathbf{P}_{\pi^+} - \mathbf{P}_{\pi^-})/2$. The azimuthal angle ϕ_R is defined through the plane formed by the spatial component of \mathbf{R} orthogonal to \mathbf{P}_h

$$\mathbf{R}_T = \mathbf{R} - (\mathbf{R} \cdot \hat{\mathbf{P}}_h) \hat{\mathbf{P}}_h , \quad (5)$$

and the virtual photon direction, *i.e.*

$$\phi_R = \frac{(\mathbf{q} \times \mathbf{k}) \cdot \mathbf{R}_T}{|(\mathbf{q} \times \mathbf{k}) \cdot \mathbf{R}_T|} \arccos(\hat{n}_{\text{lept}} \cdot \hat{n}_{\text{had}}) . \quad (6)$$

The azimuthal angle ϕ_h is defined through the plane formed by \mathbf{P}_h and the direction of the virtual photon and will be important for the study of acceptance effects. Both angles, ϕ_h and ϕ_R , correspond to the definitions given in Ref. [14].

Each SF has two subscripts indicating the polarization of the beam and target, respectively, and can be written in terms of simple products of a PDF and a di-hadron fragmentation function (FF). The SFs depend on the Bjorken variable x (through the PDF) and on the fraction of the virtual photon energy carried by the two hadrons $z = z_{\pi^+} + z_{\pi^-}$, the pion pair invariant mass $m_{\pi^+\pi^-}$ and $\cos \theta$ (through the FF). Here, θ is the angle between the direction of one of the final state hadrons in the pair center-of-mass frame and the direction of their centre-of-mass in the photon-target rest frame. The PDFs and FFs depend also on Q^2 , through the kinematical suppression

of the twist-3 contributions, as well as the QCD evolution equations.

The unpolarized cross section is proportional to the product of the unpolarized PDF $f_1(x)$ and the unpolarized di-hadron FF D_1 . We neglect here the structure function $F_{UU}^{\cos \phi_R}$, which is considered in the systematic uncertainty evaluation only. The two terms appearing in the polarized structure function $F_{LU}^{\sin \phi_R}$ are both the product of a leading-twist function and a twist-3 one, which could equally contribute. In Eq. (2), $e(x)$ appears coupled to the *chiral-odd* interference fragmentation function (IFF) H_1^{\triangleleft} [13].

In the di-hadron framework [15, 16], the hadron pair is assumed to be mainly produced in a relative s - or p -wave channel. Therefore, it is convenient to expand the $\cos \theta$ dependence of the IFF in a partial wave series that can be truncated to the first-order terms. This allows for example to replace the IFF $H_1^{\triangleleft}(z, \cos \theta, m_{\pi^+\pi^-})$ in Eq. (2) with the leading term of the partial wave expansion $H_{1,sp}^{\triangleleft}(z, m_{\pi^+\pi^-})$, which has been extracted [17–19] from Belle data [20].

The analysis we present in this letter is based on the data collected in Hall B of Jefferson Laboratory in 2003 by impinging a 5.498 GeV longitudinally polarized electron beam on a 5-cm long unpolarized liquid-hydrogen target. The CEBAF Large Acceptance Spectrometer (CLAS) [21] was used to detect the scattered electron and two oppositely charged pions of the reaction $ep \rightarrow e\pi^+\pi^-X$. The final di-hadron sample is defined through specific DIS cuts. To be in the scaling regime, the virtuality of the exchanged photon is required to be $Q^2 > 1 \text{ GeV}^2$ and, in order to avoid the resonance region, we impose $W > 2 \text{ GeV}$. The cut $y < 0.85$ is then applied to suppress radiative events. Pions coming from the current-fragmentation region were selected by applying on each pion the cut $x_F > 0$, where the Feynman- x variable is defined as $x_F = 2p_{\parallel}/W$, with p_{\parallel} the pion pair four-momentum component parallel to the virtual-photon direction. Exclusive events are removed through a cut on the missing mass $m_{e\pi^+\pi^-X} > 1.05 \text{ GeV}$. Spurious contaminations from exclusive baryonic resonance production (for example $\Delta^{++}\pi^- \rightarrow p\pi^+\pi^-$) have been studied through Monte Carlo simulations and are further suppressed at the few percent level by cutting on the energy fraction of the pions, namely $z_{\pi^+} > 0.28$ and $z_{\pi^-} > 0.25$.

Experimentally, the BSA is defined as

$$A_{LU} = \frac{1}{P_B} \frac{(N_+ - N_-)}{(N_+ + N_-)} , \quad (7)$$

where $N_{+(-)}$ are the number of counts corresponding to each beam-helicity state, and $P_B = 0.75 \pm 0.02$ is the average beam polarization over the entire data taking period. The BSA has been computed in one dimensional projections as a function of x , z , $m_{\pi^+\pi^-}$ and Q^2 and integrating over all the other kinematic variables.

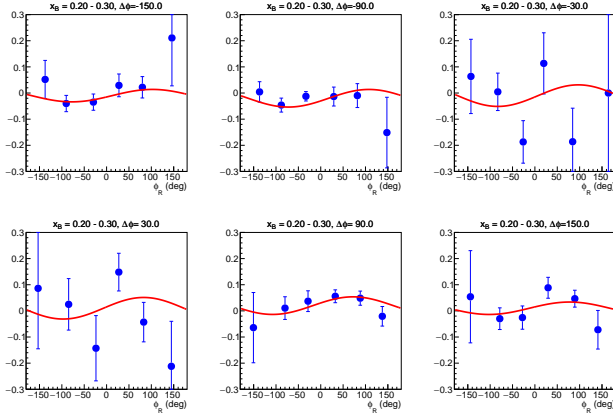


FIG. 1. (Color online) BSA as a function of ϕ_R in the 6 $\Delta\phi$ bins from -180° to 180° for the bin $x = 0.2 \div 0.3$. The full circles represent the experimental measurement with the vertical bar indicating the total uncertainty, while the curves represent the result of the fit with Eq. (8).

From the theoretical point of view, the only surviving azimuthal modulation of the BSA is the $\sin \phi_R$ moment of Eq. (1). However, kinematic correlations due to the limited phase space available in real data and non-uniform detector acceptance might lead to incomplete cancellation of modulations involving transverse momentum dependent functions [16]. A detailed study based on Monte Carlo simulations demonstrated that a reliable extraction of the $A_{LU}^{\sin \phi_R}$ moment can be achieved by binning the data in a 6×6 matrix in the two angles ϕ_R and $\Delta\phi = \phi_h - \phi_R$, and performing a 2D fit with the function

$$A_{LU} = A_{LU}^{\sin \phi_R} \sin \phi_R + A_{LU}^{\sin(\phi_h - \phi_R)} \sin(\phi_h - \phi_R) + A_{LU}^{\sin \phi_h} \sin \phi_h , \quad (8)$$

representing the relevant modulations from the cross section.

An example of the 2D fit in the bin $x = 0.2 \div 0.3$ is shown in Fig. 1. Each panel represents one $\Delta\phi$ bin, the points show the ϕ_R dependence of the measured BSA. The curve is the result of the 2D fit. The fit has been performed considering the total (statistical and systematic) point-to-point uncertainty shown by the error bars. The systematic uncertainty, amounting to 30%, is due to the truncation in the partial wave expansion of the di-hadron FFs. It has been estimated by taking into account the average values of the θ -harmonics of the series from the experimental data and conservatively assuming that the FFs associated to higher harmonics are of the same order of magnitude as the leading one.

The $A_{LU}^{\sin \phi_R}$ fitted moments are shown in Fig. 2 as a function of x and Q^2 . The projections for z and $m_{\pi^+\pi^-}$ are given in Fig. 3. The solid circles correspond to data points. The error bars show the statistical uncertainties from the fits. At the bottom of each plot, the gray band represents the total systematic uncertainty, which includes: a 3% contribution due to the electron beam

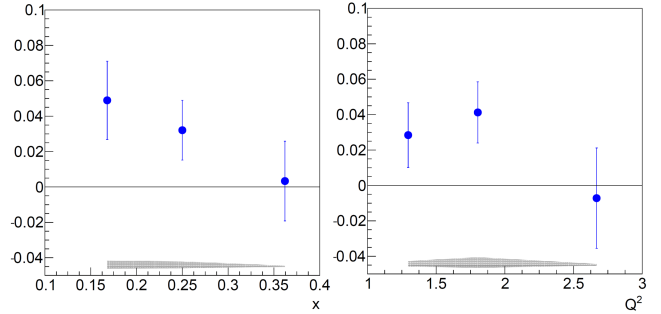


FIG. 2. (Color online) Dependence on x (l.h.s.) and Q^2 (r.h.s.) of the $\sin \phi_R$ moment $A_{LU}^{\sin \phi_R}$ of the beam spin asymmetry. The error bars and the gray band represents the statistical and systematic uncertainties.

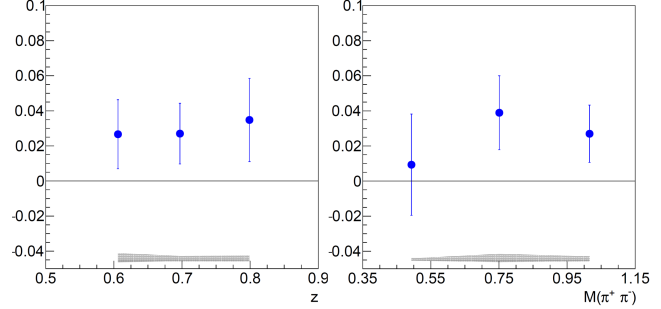


FIG. 3. (Color online) Dependence on z (l.h.s.) and $m_{\pi\pi}$ (r.h.s.) of the $\sin \phi_R$ moment $A_{LU}^{\sin \phi_R}$ of the Asymmetry. The error bars and the gray band represents the statistical and systematic uncertainties.

polarization; a 3% contribution due to the radiative corrections; the residual contamination from baryon resonance decays, estimated from Monte Carlo studies to be between 2 and 9% depending on the kinematics.

The kinematic bins in the figures have been chosen so that they have approximately the same statistics, except for $m_{\pi^+\pi^-}$, where the second bin covers the ρ mass region, while the first (third) bin covers the mass region before (after) the ρ mass. The average Q^2 of the data is 1.77 GeV^2 . For the x dependence of the BSA, the invariant mass values range from the threshold to $\sim 1.7 \text{ GeV}$ and $0.53 < z < 0.95$.

In this letter we report the pioneering observation of a twist-3 observable in di-hadron SIDIS; hence, no previous measurements are available for comparison. The x projection of the $\sin \phi_R$ moment reflects the behavior of the PDFs. In Fig. 4 this projection of $A_{LU}^{\sin \phi_R}$ is compared to models for the twist-3 PDF $e(x)$ —neglecting the second term on the r.h.s of Eq. (2). The curves corresponding to the different models for $e(x)$ are produced by combining to the extracted di-hadron FFs [19]. The gray-dotted band corresponds to the LFCQM of Ref. [22] together with MSTW08LO unpolarized PDF [23], the green-dashed band corresponds to the asymmetry with both PDFs evaluated in the spectator model [24], while the red-full band corresponds to the MIT bag model [25] for both $f_1(x)$ and $e(x)$.

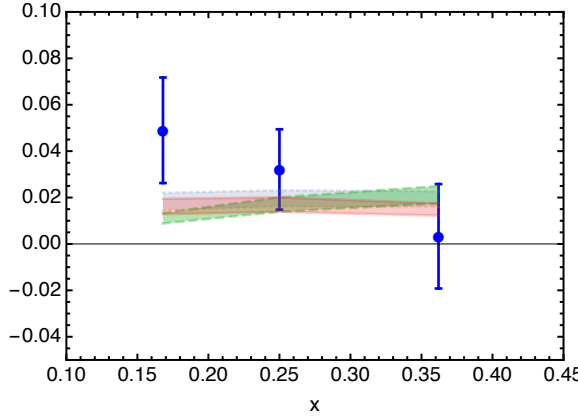


FIG. 4. (Color online) Dependence on x of the $\sin \phi_R$ moment $A_{LU}^{\sin \phi_R}$ of the beam spin asymmetry compared to model calculations: the spectator model [24] in green-dashed, the bag model [25] in red-full and the gray-dotted band corresponds to the LFCQM [22], all using the di-hadron FFs [19].

Other calculations, not shown in the figure, have been proposed [26–28]. The models are consistent among themselves; they are in agreement with the experimental data within about 1σ , although the data seems to indicate a steeper decrease at high x than the models. The behavior of the three points could be examined in a thorough point-by-point extraction of $e(x)$ [29], as has been sketched in Ref. [30] using preliminary results from the same CLAS data we present in this letter.

In summary, for the first time a beam spin asymmetry for the semi-inclusive electroproduction of charged pion pairs has been measured. The one-dimensional projections of the moment $A_{LU}^{\sin \phi_R}$ in x , z , $m_{\pi^+\pi^-}$ and Q^2 have been extracted. This measurement constitutes a pioneering study that has accounted for systematic sources of uncertainties that were shown to have little impact on the present results but that would be crucial for ongoing studies of di-hadron observables using the CLAS12 [31] detector with proton and deuteron targets [32], at an order of magnitude higher luminosity, which will provide further information on the twist-3 nucleon structure in the mid- x region.

The invariant mass distributions of di-hadrons from different SIDIS and e^+e^- experiments indicate that a very significant fraction of inclusive pions are coming from correlated di-hadrons. The observables for pions from decays of vector mesons have peculiar spin and momentum dependences and may require different radiative corrections, modeling, and interpretation of observables sensitive to the transverse momentum of quarks [33]. As such, di-hadron measurements establish the bases for future experimental and phenomenological studies.

We thank the staff of the Accelerator and Physics Divisions for making the experiment possible. Special thanks

to A. Bacchetta, B. Pasquini, M. Polyakov, M. Radici, P. Schweitzer and M. Wakamatsu for useful discussions. This work was supported in part by the U.S. Department of Energy (No. DE-FG02-96ER40950) and National Science Foundation, the French Centre National de la Recherche Scientifique and Commissariat à l’Energie Atomique, the French-American Cultural Exchange (FACE), the Italian Istituto Nazionale di Fisica Nucleare, the Chilean Comisión Nacional de Investigación Científica y Tecnológica (CONICYT), the Mexican Consejo Nacional de Ciencias y Tecnología (CONACyT), the National Research Foundation of Korea, and the UK Science and Technology Facilities Council (STFC). A.C. is supported by DGAPA-PAPIIT IA101720 and CONACyT Ciencia de Frontera 2019 No. 51244 (FORDECYT-PRONACES). The Jefferson Science Associates (JSA) operates the Thomas Jefferson National Accelerator Facility for the United States Department of Energy under contract DE-AC05-06OR23177.

-
- [1] R. L. Jaffe and X. D. Ji, Nucl. Phys. B **375** (1992) 527. doi:10.1016/0550-3213(92)90110-W
 - [2] A. Efremov and P. Schweitzer, JHEP **08** (2003), 006 doi:10.1088/1126-6708/2003/08/006 [arXiv:hep-ph/0212044 [hep-ph]].
 - [3] M. Burkhardt, Phys. Rev. D **88** (2013) 114502 doi:10.1103/PhysRevD.88.114502 [arXiv:0810.3589 [hep-ph]].
 - [4] C. Y. Seng, Phys. Rev. Lett. **122** (2019) no.7, 072001 doi:10.1103/PhysRevLett.122.072001 [arXiv:1809.00307 [hep-ph]].
 - [5] J. R. Ellis, K. A. Olive and C. Savage, Phys. Rev. D **77** (2008) 065026 doi:10.1103/PhysRevD.77.065026 ; [arXiv:0801.3656 [hep-ph]]; T. Bhattacharya, V. Cirigliano, S. D. Cohen, A. Filipuzzi, M. Gonzalez-Alonso, M. L. Graesser, R. Gupta and H. W. Lin, Phys. Rev. D **85** (2012) 054512 doi:10.1103/PhysRevD.85.054512 ; [arXiv:1110.6448 [hep-ph]]; M. Cirelli, E. Del Nobile and P. Panci, JCAP **1310** (2013) 019 doi:10.1088/1475-7516/2013/10/019. [arXiv:1307.5955 [hep-ph]].
 - [6] A. Courtoy, S. Baessler, M. Gonzalez-Alonso and S. Liuti, Phys. Rev. Lett. **115** (2015) 162001 doi:10.1103/PhysRevLett.115.162001 [arXiv:1503.06814 [hep-ph]] ; T. Liu, Z. Zhao and H. Gao, Phys. Rev. D **97** (2018) no.7, 074018 doi:10.1103/PhysRevD.97.074018 [arXiv:1704.00113 [hep-ph]].
 - [7] A. Airapetian *et al.* [HERMES], Phys. Lett. B **648** (2007), 164–170 doi:10.1016/j.physletb.2007.03.015 [arXiv:hep-ex/0612059 [hep-ex]].
 - [8] W. Gohn *et al.* [CLAS], Phys. Rev. D **89** (2014) no.7, 072011 doi:10.1103/PhysRevD.89.072011 [arXiv:1402.4097 [hep-ex]].
 - [9] H. Avakian *et al.* [CLAS], Phys. Rev. D **69** (2004), 112004 doi:10.1103/PhysRevD.69.112004 [arXiv:hep-ex/0301005 [hep-ex]].
 - [10] M. Aghasyan *et al.*, Phys. Lett. B **704** (2011) 397 doi:10.1016/j.physletb.2011.09.044 [arXiv:1106.2293 [hep-ex]] .

- [11] A. Moretti [COMPASS], PoS **SPIN2018** (2019), 052 doi:10.22323/1.346.0052 [arXiv:1901.01773 [hep-ex]].
- [12] A. Efremov, K. Goeke and P. Schweitzer, Phys. Rev. D **67** (2003), 114014 doi:10.1103/PhysRevD.67.114014 [arXiv:hep-ph/0208124 [hep-ph]].
- [13] A. Bacchetta and M. Radici, Phys. Rev. D **69** (2004), 074026 doi:10.1103/PhysRevD.69.074026 [arXiv:hep-ph/0311173 [hep-ph]].
- [14] S. Gliske, A. Bacchetta and M. Radici, Phys. Rev. D **90** (2014) no.11, 114027 Erratum: [Phys. Rev. D **91** (2015) no.1, 019902] doi:10.1103/PhysRevD.90.114027, 10.1103/PhysRevD.91.019902 [arXiv:1408.5721 [hep-ph]].
- [15] A. Bianconi, S. Boffi, R. Jakob and M. Radici, Phys. Rev. D **62** (2000), 034008 doi:10.1103/PhysRevD.62.034008 [arXiv:hep-ph/9907475 [hep-ph]].
- [16] A. Bacchetta and M. Radici, Phys. Rev. D **67** (2003), 094002 doi:10.1103/PhysRevD.67.094002 [arXiv:hep-ph/0212300 [hep-ph]].
- [17] A. Bacchetta, A. Courtoy and M. Radici, JHEP **1303** (2013) 119 doi:10.1007/JHEP03(2013)119 [arXiv:1212.3568 [hep-ph]].
- [18] M. Radici, A. Courtoy, A. Bacchetta and M. Guagnelli, JHEP **05** (2015), 123 doi:10.1007/JHEP05(2015)123 [arXiv:1503.03495 [hep-ph]].
- [19] A. Courtoy, A. Bacchetta, M. Radici and A. Bianconi, Phys. Rev. D **85** (2012), 114023 doi:10.1103/PhysRevD.85.114023 [arXiv:1202.0323 [hep-ph]].
- [20] A. Vossen *et al.* [Belle], Phys. Rev. Lett. **107** (2011), 072004 doi:10.1103/PhysRevLett.107.072004 [arXiv:1104.2425 [hep-ex]].
- [21] B.A. Mecking *et al.*, Nucl. Instr. Meth. **A503**, 513 (2003).
- [22] B. Pasquini and S. Rodini, Phys. Lett. B **788** (2019) 414 doi:10.1016/j.physletb.2018.11.033 [arXiv:1806.10932 [hep-ph]].
- [23] A. D. Martin, W. J. Stirling, R. S. Thorne and G. Watt, Eur. Phys. J. C **63** (2009) 189 [arXiv:0901.0002 [hep-ph]].
- [24] R. Jakob, P. J. Mulders and J. Rodrigues, Nucl. Phys. A **626** (1997) 937 doi:10.1016/S0375-9474(97)00588-5 [hep-ph/9704335].
- [25] A. I. Signal, Nucl. Phys. B **497** (1997) 415 [hep-ph/9610480]; R. L. Jaffe and X. D. Ji, Nucl. Phys. B **375** (1992) 527. doi:10.1016/0550-3213(92)90110-W
- [26] Y. Ohnishi and M. Wakamatsu, Phys. Rev. D **69** (2004) 114002 [hep-ph/0312044] ; M. Wakamatsu, Phys. Lett. B **509** (2001) 59 doi:10.1016/S0370-2693(01)00200-3 [hep-ph/0012331].
- [27] P. Schweitzer, Phys. Rev. D **67** (2003) 114010 doi:10.1103/PhysRevD.67.114010 [hep-ph/0303011].
- [28] C. Lorcé, B. Pasquini and P. Schweitzer, JHEP **1501** (2015) 103 doi:10.1007/JHEP01(2015)103 [arXiv:1411.2550 [hep-ph]].
- [29] A. Avakian, A. Courtoy, M. Mirazita, S. Pisano, in progress.
- [30] A. Courtoy, “Insights into the higher-twist distribution $e(x)$ at CLAS,” arXiv:1405.7659 [hep-ph].
- [31] V. D. Burkert *et al.* Nucl.Instrum.Meth.A **959** (2020) 163419.
- [32] S. Pisano *et. al.*, JLab Experiment E12-06-112B, E12-09-008B (2014).
- [33] H. Avakian [CLAS], PoS **DIS2019** (2019), 265 doi:10.22323/1.352.0265

SUPPLEMENTAL MATERIAL

We provide in this Section Tables that support the main part of the manuscript. In Table I, the kinematic ranges for the relevant variables are given. The full kinematic ranges are given in Tables II, IV, VI and VIII; the asymmetries, statistical and systematical uncertainties are provided for each 1D projection in Tables III, V, VII and IX.

Variable	Bin 1	Bin 2	Bin 3
x	$0.114 \div 0.200$	$0.200 \div 0.300$	$0.300 \div 0.593$
Q^2 (GeV 2)	$1.000 \div 1.500$	$1.500 \div 2.200$	$2.200 \div 4.644$
z	$0.530 \div 0.650$	$0.650 \div 0.750$	$0.705 \div 0.948$
$m_{\pi^+\pi^-}$ (GeV)	$0.279 \div 0.650$	$0.650 \div 0.852$	$0.852 \div 1.734$

TABLE I. Bins of the 1D projections of the $A_{LU}^{\sin \phi_R}$ measurements for each of the respective projections.

bin	x			Q^2 (GeV 2)			z			$m_{\pi^+\pi^-}$ (GeV)		
	min	max	ave	min	max	ave	min	max	ave	min	max	ave
1	0.114	0.200	0.168	1.000	1.752	1.279	0.531	0.948	0.692	0.279	1.734	0.826
2	0.200	0.300	0.250	1.084	2.628	1.673	0.530	0.933	0.691	0.279	1.627	0.718
3	0.300	0.593	0.362	1.356	4.644	2.353	0.531	0.913	0.680	0.279	1.384	0.626

TABLE II. Kinematic ranges of the three x bins.

Bin	$\langle x \rangle$	$A_{LU}^{\sin \phi_R}(x)$	Stat	Syst
1	0.168	0.0490	0.0221	0.0054
2	0.250	0.0321	0.0169	0.0038
3	0.362	0.0033	0.0225	0.0004

TABLE III. Asymmetries for the x projection.

bin	x			Q^2 (GeV 2)			z			$m_{\pi^+\pi^-}$ (GeV)		
	min	max	ave	min	max	ave	min	max	ave	min	max	ave
1	0.114	0.324	0.197	1.000	1.500	1.296	0.531	0.948	0.693	0.279	1.734	0.748
2	0.171	0.412	0.274	1.500	2.200	1.803	0.530	0.938	0.688	0.279	1.627	0.704
3	0.251	0.593	0.374	2.200	4.644	2.668	0.531	0.924	0.678	0.279	1.492	0.673

TABLE IV. Kinematic ranges of the three Q^2 bins.

Bin	$\langle Q^2 \rangle$ (GeV 2)	$A_{LU}^{\sin \phi_R}(Q^2)$	Stat	Syst
1	1.296	0.0284	0.0183	0.0032
2	1.803	0.0412	0.0173	0.0051
3	2.668	-0.0072	0.0284	0.0009

TABLE V. Asymmetries for the Q^2 projection.

	x			Q^2 (GeV 2)			z			$m_{\pi^+\pi^-}$ (GeV)		
bin	min	max	ave	min	max	ave	min	max	ave	min	max	ave
1	0.114	0.593	0.271	1.000	4.588	1.834	0.530	0.650	0.606	0.279	1.383	0.660
2	0.114	0.592	0.272	1.000	4.644	1.820	0.650	0.750	0.697	0.279	1.653	0.727
3	0.114	0.551	0.255	1.000	4.176	1.723	0.750	0.948	0.799	0.279	1.734	0.770

TABLE VI. Kinematic ranges of the three z bins.

Bin	$< z >$	$A_{LU}^{\sin \phi_R}(z)$	Stat	Syst
1	0.606	0.0267	0.0197	0.0037
2	0.697	0.0270	0.0173	0.0031
3	0.799	0.0348	0.0237	0.0039

TABLE VII. Asymmetries for the z projection.

	x			Q^2 (GeV 2)			z			$m_{\pi^+\pi^-}$ (GeV)		
bin	min	max	ave	min	max	ave	min	max	ave	min	max	ave
1	0.114	0.593	0.291	1.000	4.644	1.865	0.530	0.933	0.676	0.279	0.650	0.493
2	0.114	0.590	0.267	1.000	4.588	1.805	0.531	0.940	0.687	0.650	0.852	0.751
3	0.114	0.550	0.231	1.000	4.344	1.705	0.531	0.948	0.706	0.850	1.734	1.016

TABLE VIII. Kinematic ranges of the three $m_{\pi^+\pi^-}$ bins.

Bin	$< m_{\pi^+\pi^-} >$ (GeV)	$A_{LU}^{\sin \phi_R}(m_{\pi^+\pi^-})$	Stat	Syst
1	0.493	0.0093	0.0289	0.0012
2	0.751	0.0389	0.0211	0.0045
3	1.016	0.0270	0.0163	0.0030

TABLE IX. Asymmetries for the $m_{\pi^+\pi^-}$ projection.